Front. Optoelectron. 2019, 12(2): 148–156
https://doi.org/10.1007/s12200-018-0846-5

RESEARCH ARTICLE

On-chip programmable pulse processor employing cascaded MZI-MRR structure

Yuhe ZHAO*, Xu WANG*, Dingshan GAO, Jianji DONG (✉), Xinliang ZHANG

Wuhan National Laboratory for Optoelectronics, School of Optical and Electronic Information, Huazhong University of Science and Technology, Wuhan 430074, China

Abstract Optical pulse processor meets the urgent demand for high-speed, ultra wideband devices, which can avoid electrical confinements in various fields, e.g., all-optical communication, optical computing technology, coherent control and microwave fields. To date, great efforts have been made particularly in on-chip programmable pulse processing. Here, we experimentally demonstrate a programmable pulse processor employing 16-cascaded Mach-Zehnder interferometer coupled microring resonator (MZI-MRR) structure based on silicon-on-insulator wafer. With micro-heaters loaded to the device, both amplitude and frequency tunings can be realized in each MZI-MRR unit. Thanks to its reconfigurability and integration ability, the pulse processor has exhibited versatile functions. First, it can serve as a fractional differentiator whose tuning range is $0.51-2.23$ with deviation no more than 7%. Second, the device can be tuned into a programmable optical filter whose bandwidth varies from 0.15 to 0.97 nm. The optical filter is also shape tunable. Especially, 15-channel wavelength selective switches are generated.

Keywords integrated optics devices, optical processing, all-optical devices, pulse shaping

1 Introduction

With the crying needs for ultra-fast pulse processing along with ever-increasing communication capacity, traditional pulse processing with electrical devices has difficulty in meeting the growing sampling rate and frequency band, due to intrinsic restriction from electronic bottleneck [1]. All-optical pulse processing takes advantages of its fast processing rate, broader carrier bandwidth, lower power dissipation and immunity to electromagnetic interference [2–4]. Optical pulse processing is the method to transform a pulse either in time domain or in frequency domain, to change its amplitude, phase, frequency or inter-pulse separation, therefore there are three mainstream derived approaches [4]: temporal synthesis [4–9], Fourier synthesis [10–15] and frequency-to-time mapping [16–21]. For the past few decades optical processing has been providing viable applications, such as, optical filters [8], optical integrators [22], optical differentiators [23,24], delay lines [25–27], dispersion compensation [28,29], optical frequency combs [30], and optical arbitrary waveform generation (OAWG) [24,31]. Besides, in optical communication field, optical processing copes with bit pattern recognition [32] and optical time division multiplexing (OTDM) [33]. Microwave arbitrary waveform generation [16,21], radiofrequency (RF) filter [34,35] and beam forming [36,37] for microwave application are also counted, in view of the similar means by which we dealing with optical and microwave signals.

At the very beginning, to tailor the spectrum of the signal, people employed discrete device such as masks and spatial light modulators [10]. Whereafter, fiber Bragg gratings (FBGs) [7,17,38,39] played an important role in pulse processing. Thanks to its compactness, stability, and complementary metal-oxide-semiconductor (CMOS)-compatibility, silicon photonics was believed to be a great advance in pulse processing field [40]. Among all these integrated components, there are some typical elements including arrayed waveguide gratings [13, 41,42], on-chip gratings [43], and microrings [18,44,45]. In recent years, significant efforts have been made in fully reconfigurable pulse shaper [9,18,27,46–50], which is ongoing and to be focused more and more in the future. The trends about where to go is forecasted to be system-on-a-chip with full reconfigurability.

Received July 8, 2018; accepted August 10, 2018

E-mail: jjdong@hust.edu.cn

*These authors contributed equally to this work

In this paper, we proposed an optical pulse processor in form of 16-cascaded Mach-Zehnder interferometer coupled microring resonator (MZI-MRR) structure based on photonic integrated circuit. The chip was presented on silicon-on-insulator (SOI) platform, and it is packaged with a printed circuit board (PCB) with electrodes. Due to the wide tunability for both Mach-Zehnder interferometer arms and ring resonators, the transmission of this optical filter is highly reconfigurable, being broadly applicable to numerous applications and fields in optical pulse processing and microwave signal generation. We have demonstrated a variety of applications with this pulse processor, including fractional differentiator with wide tuning range and a programmable optical filter. Our scheme is a promising candidate nowadays in pulse processing due to its wide reconfigurability, on-chip integration, CMOS-compatibility and low power consumption.

2 Operation principle and device fabrication

The design of our optical pulse processor is shown in Fig. 1, which is based on an SOI wafer. The pulse processor consists of 16 cascaded microrings, each of which is coupled with an MZI arm. The spectral response of each microring is shown as [51,52]

$$t=\frac{\sqrt{1-\kappa_1^2}-\alpha\sqrt{1-\kappa_2^2}\mathrm{e}^{\mathrm{j}\varphi}}{1-\alpha\sqrt{1-\kappa_1^2}\sqrt{1-\kappa_2^2}\mathrm{e}^{\mathrm{j}\varphi}}, \tag{1}$$

where α is the round-trip intrinsic power loss of the resonator, κ_1 and κ_2 are the power coupling rate for the input and output waveguide, and φ is the round-trip phase shift. In our case, we replace the input straight waveguides for the MZI arms above the microrings, as a result, the couple region of MZI arm and microring can be considered as a whole MZI. Thus the power coupling rate κ_1 is written as below

$$\kappa_1=\kappa_0(1-\kappa_0)\times[t_\mathrm{b}+t_\mathrm{r}-2\sqrt{t_\mathrm{b}t_\mathrm{r}}\cos(\varphi_\mathrm{b}-\varphi_\mathrm{r})], \tag{2}$$

where κ_0 is the power coupling rate between MZI arms and microrings, t_b, t_r and φ_b, φ_r are the transmission coefficient and phase shift of MZI arm and ring arm, respectively.

In our case, the ultimate frequency response of cascaded MZI-MRRs is the product of each of them. Notably, since there is feedback from the drop-port, the microring transmission should be written as 2 × 2 transfer matrix. Considering the feedback is complementary to the through port, we can ignore the feedback and consider only the response of through port here. Therefore, with Eqs. (1) and (2), the spectral response of the MZI-MRR structure is expressed as

$$t=\prod_{i=1}^{16}\frac{\sqrt{1-\kappa_{1i}^2}-\alpha\sqrt{1-\kappa_{2i}^2}\mathrm{e}^{\mathrm{j}\varphi_i}}{1-\alpha\sqrt{1-\kappa_{1i}^2}\sqrt{1-\kappa_{2i}^2}\mathrm{e}^{\mathrm{j}\varphi_i}}, \tag{3}$$

where κ_{1i} and κ_{2i} are the power coupling rate of the i-th ring resonator for the input and output waveguide, and φ_i is the round-trip phase shift of the i-th ring resonator.

With a micro-heater adjusting the effective refractive index of MZI arm, the dip depth of the microring notch filter is tunable. There is a micro-heater above the microring as well, which ensures the tunability of the resonant wavelength of the ring resonator. Thus due to thermo-optic effect, a pair of micro-heaters, including one on the MZI arm to adjust φ_b and the other on the microring to adjust φ, can provide tunability for both the depth and the frequency of the notch. The dual-parameter control for the dips is applied to tailor the optical spectrum into any target shape, making it possible to be applicable in a variety of fields. With Eq. (3), we can theoretically calculate the target spectral response for this device, which allows us to pre-design the voltages of the electrodes. As a trade-off between tunability and power consumption, we choose microring units as many as 16. When the interval between each channel is 50 GHz, the bandwidth can reach ~6 nm. Besides, the microrings are divided into four groups and each group has four identical rings. There is a tiny deviation of ring radii of 10 nm between each group, which makes it easier to identify each

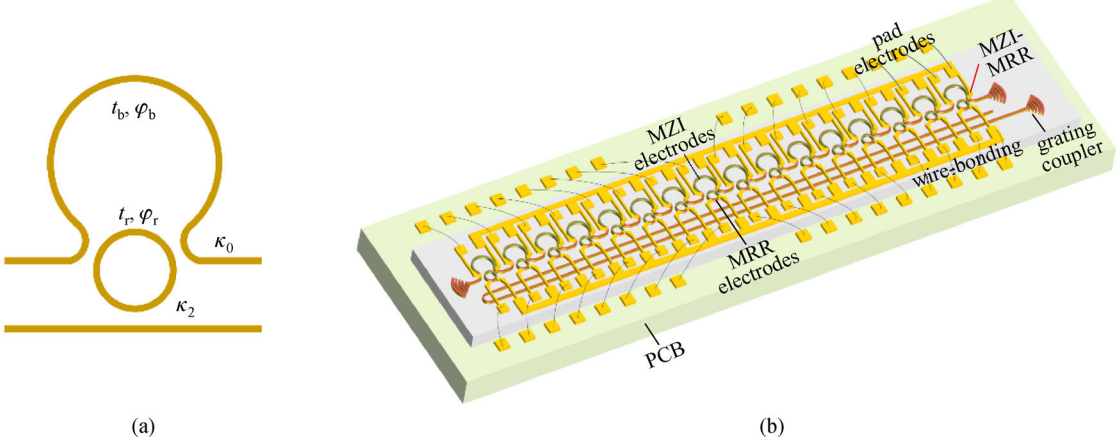

Fig. 1 Schematics of 16-cascaded MZI-MRR optical filter on SOI wafer

notches in the frequency domain.

The chip is fabricated on an SOI wafer using a multi project wafer passive process flow, and the microscopic image is shown in Fig. 2(a). The waveguide is 220 nm top silicon with 3 μm buried oxide substrate. Except for the grating couplers, the rest of waveguide is strip waveguide with 220 nm silicon. The waveguide pattern is transferred to the hard mask through 248 nm deep UV lithography and etched. The grating coupler is fan shaped with 70 nm-thick shallow etching. As for the MZI-MRR part, the MZI arcs are 174 μm-long, while the microrings have a radius of 8 μm. After the waveguide was covered by deposition of 1.2 μm silica isolated layer, there are 32 arc-shape micro-heaters made of 120 nm-thick TiN, working with thermo-optic effect to change the refractive index of the waveguide. The whole chip is packaged on a PCB via wire-bonding technology. There are 16 × 2 electrodes for micro-heaters with a common ground. Figures 2(b)–2(d) show more details with zoomed in microscopic image.

The spectral transmission of the device is tested using a broadband light source. The total loss for the fiber-to-fiber transmission is about 11 dB. The bandwidth of through port of a single microring resonator is 0.09 nm. Different voltages are exerted to either electrodes of MZI arc regions or electrodes of ring resonators to confirm the changes in spectral response, and the measured resistances are 1.7 and 0.9 kΩ, respectively. Figure 3(a) shows the transmission power of one unit for the ring array. By changing the applied voltages, the extinction ratio (ER) of the resonant wavelength varies from 0 to 17 dB, indicating 12.0 mW power dissipation for π shift. Figure 3(b) shows that the redshift of resonant wavelength with 5.6 nm when voltages of ring resonators change from 1.1 to 3.2 V. As we can see, both resonant ER and central wavelength can be successfully tuned by a pair of heaters. Then all the 16 ring units can be tailored with their spectra one-by-one to manage the whole spectral shape.

3 Experimental result

3.1 Dynamic fractional differentiator

Optical temporal differentiator, as an important device in all-optical circuits, has been intensively investigated in all-optical computing, pulse coding, and optical pulse shaping, etc. An optical temporal differentiator handles the complex envelope of an input pulse, obtaining its n-th order time derivative [53,54]. By tuning the voltages of electrodes, the chip transmission can be configured into the target shape. In this section, a fractional differentiator covering differential order from 0.51 to 2.23 has been realized, with 4 notches aligned to common central angular frequency ω_0 of input optical signal.

The experimental setup of differentiator is shown in Fig. 4. To generate a short pulse, a tunable laser diode (TLD) is applied as the optical source, which is continuous wave in time domain and set at central angular frequency of 4 accordant notches, namely ω_0. A polarization controller (PC) is used to adjust the polarization of the

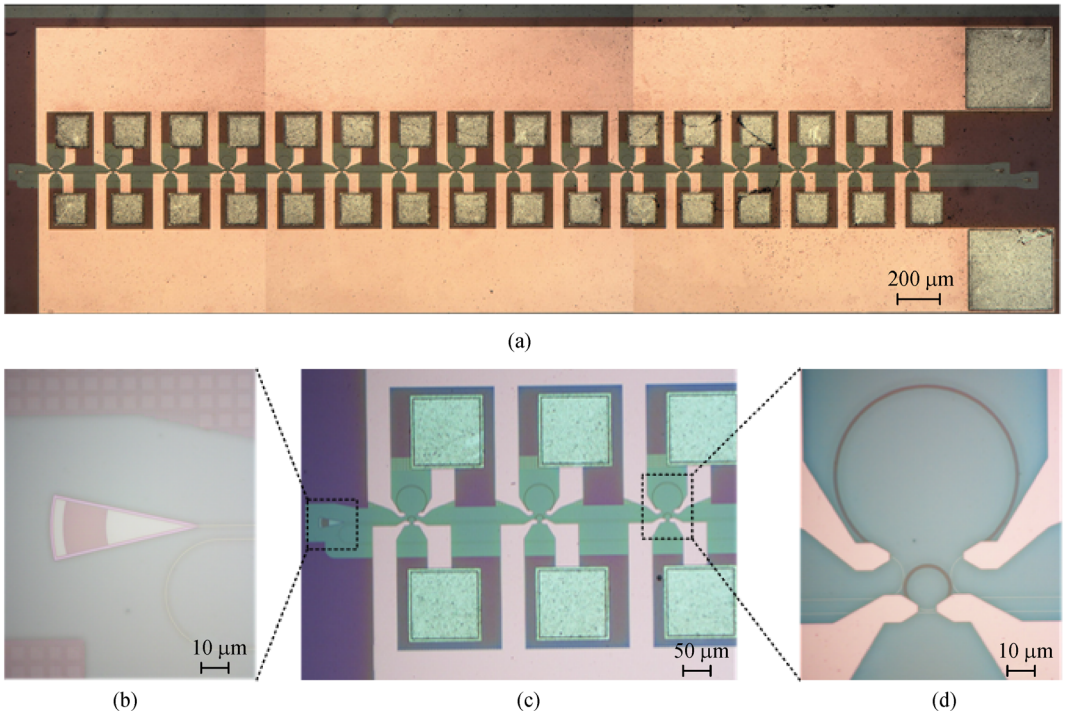

Fig. 2 (a) Microscopic image of the pulse shaper. Zoomed in microscopic picture of (b) the grating coupler, (c) the waveguide, (d) the MZI-MRR structure

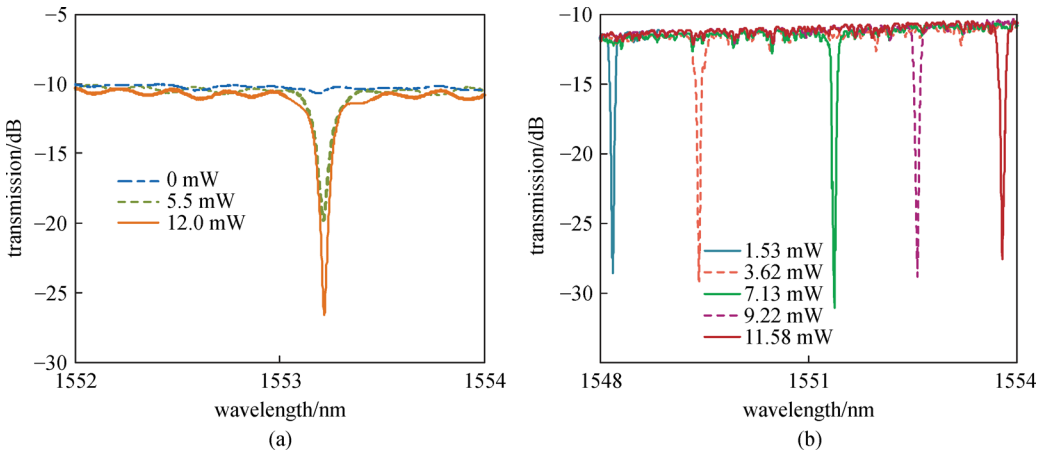

Fig. 3 (a) Transmission power of the device when different voltages are applied to arc electrodes and (b) rings electrodes

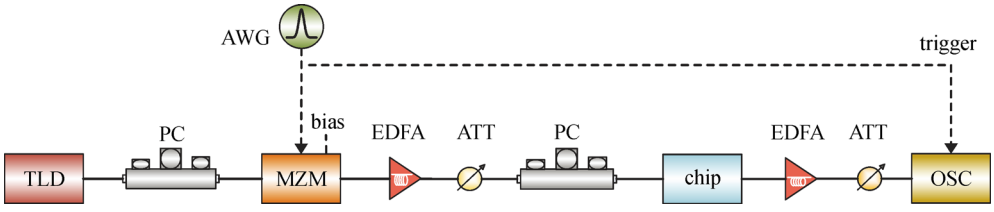

Fig. 4 Experimental setup of the differentiator employing the programmable pulse shaper. TLD: tunable laser diode, PC: polarization controller, MZM: Mach-Zehnder modulator, AWG: arbitrary waveform generator, EDFA: Erbium doped optical fiber amplifier, ATT: attenuator, OSC: oscilloscope

light as the modulator is polarization sensitive. The light is then sent into a MZM by a periodical Gaussian pulse generated by a microwave arbitrary waveform generator (AWG). In our case, the pulse period is 200 ps, and its full width at half maximum (FWHM) is 42 ps. After going through an Erbium doped fiber amplifier (EDFA) and an attenuator (ATT), the polarization is controlled by another PC before sent into the chip. As the signal wavelength is aligned to notch filters, the operation bandwidth of the differentiator is within the MRR bandwidth. After propagating in the chip, the repetitive pulse is sent into an optical sampling oscilloscope (OSC) which is synchronized with the electrical source.

Transfer functions for differentiators with varied differential order can be calculated as

$$H(\omega) = [\mathrm{j}(\omega - \omega_0)]^N, \tag{4}$$

where ω is optical angular frequency near the central angular frequency ω_0, while N is the differential order. Figures 5(a)–5(c) demonstrate the simulated (red dashed line) and measured (blue solid line) transfer function of 0.5-th order, first order and second order differentiators, and the active ranges of each differentiator are 20, 30, and 30 GHz, respectively.

When different voltages is applied to the microring electrodes, the transfer function changes. In other word, the differential order N changes. The measured input Gaussian pulse (blue solid line) in time domain is shown in Fig. 6(a), whose FWHM is 42 ps, while the simulated standard Gaussian pulse is drawn in red dashed line. Then the transfer functions are tuned in depth, thus differential order changes from 0.5 to 2.23, as shown in Figs. 6(b)–6(h). To evaluate the computing accuracy, the averaged error is defined as the deviation of power between measured ones and simulated ones in a single period of 200 ps. We calculated averaged error of the measured results against calculated results changing with various differential order, as shown in Fig. 7. All the errors meet our expectation as it is no more than 7%. Our differentiator has expanded the differential order compared to a single MZI-MRR [52]. Notably, as differential order changes from 0.5 to 2.23, the power consumption is between 0.5 and 54 mW. In theory, we can obtain fourth order differentiator using four cascaded MZI-MRR units. In practice, we cannot. The reason may lies in the mode split effect and insufficient phase shift at the notches. In conclusion, our fractional differentiator has many advantages compared to other differentiator. First, with electrodes, the central wavelength can be tuned, while some work without electrodes cannot [54]. Second, the tuning range of differential order is quite wider than the former work [52]. Theoretically, the maximum of differential order is equal to the number of microrings.

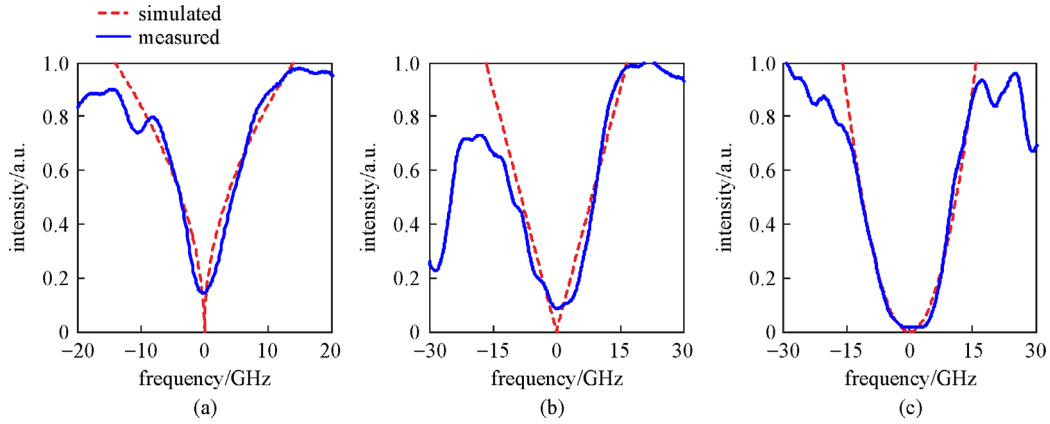

Fig. 5 Transfer function of (a) 0.5-th order, (b) first order and (c) second order

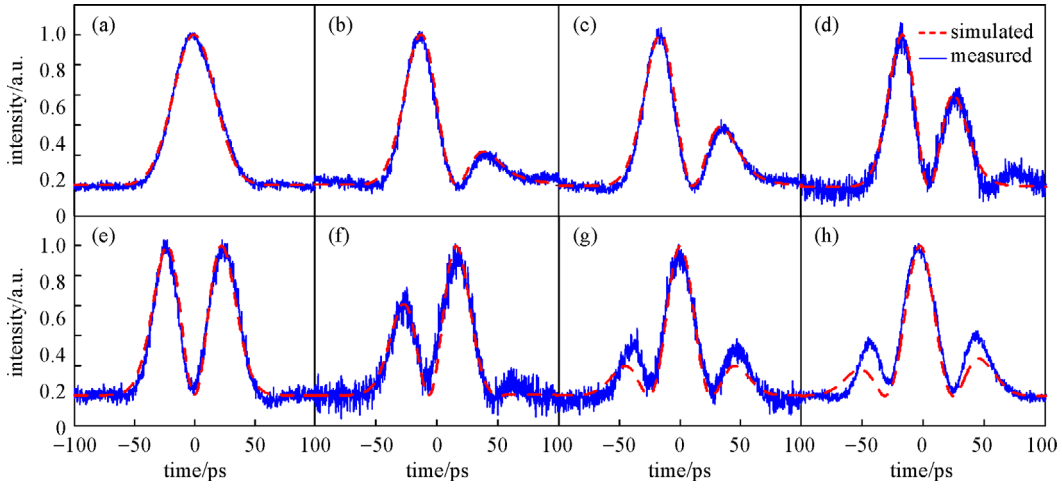

Fig. 6 Experimental results for the fractional-order differentiator based on an MZI-MRR. (a) Input pulse; (b) results of 0.51-th order; (c) 0.68-th order; (d) 0.79-th order; (e) first order; (f) 1.25-th order; (g) second order; and (h) 2.23-th order differentiator

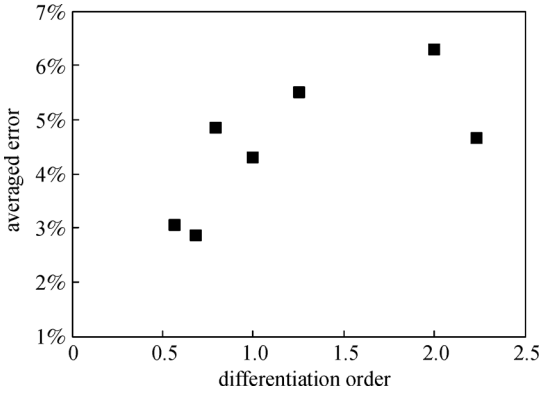

Fig. 7 Averaged error of the measured results against calculated results changing with various differential order

3.2 Programmable optical filter

Programmable optical filters play a key role in optical communication system, optical computing circuits and microwave photonics. Especially, optical filter with shape tunability, bandwidth tunability, frequency tunability gives rise to wide interests nowadays, which might be widely used in wavelength selective switches (WSS) [55]. Our pulse processor makes programmable optical filter possible since we can control the spectra for all the 16 microring units. We use a broadband optical source covering C-band as the input source. A PC is used to adjust the polarization of the light because of the polarization selectivity of the grating couplers on the chip. Direct current (DC) source acts on two probe cards to contact PCB pads, controlling the electrodes on the chip. The transmission spectrum is analyzed using an optical spectrum analyzer (OSA).

The optical filter can be both shape tunable and bandwidth tunable. First, to explore the shape tunability, we tuned the dips overlapped in frequency domain using microring heaters, and adjust the arc heaters to control the depths of each dip. Specific shapes can be calculated and simulated according to Eq. (3). Figure 8 shows transfer functions in several specific shapes, including isosceles triangle shape right angled triangle shape in Figs. 8(b) and

8(c), square shape in Fig. 8(d). Both measured and simulated results are compared. The power consumption for different shapes is around 44 mW.

To verify the bandwidth tunability, filters of square shape were demonstrated with bandwidth changing. Obviously, the more MZI-MRR works in active region, the wider square shape transfer function we will get. As shown in Fig. 9(a), the experiment started from 2 rings overlapped, where the bandwidth of the square shape transfer function is 0.15 nm. Along with more MZI-MRR units involved, the bandwidth is ever-increasing, shown in Figs. 9(b)–9(f). The bandwidths are 0.2, 0.25, 0.61, 0.83 and 0.97 nm, respectively, at the same time, the effective number of operating rings are 3, 3, 10, 13 and 15, respectively. The power consumption varies from 2 to 360 mW, while the average maximum power consumption per ring is 24 mW.

As previously mentioned, when the notches are discretely spaced with a fixed interval, the optical filter functions like a WSS. We carried out an experiment to evenly space 15 notches of MZI-MRRs along the spectra with 50 GHz grid, as shown in Fig. 10(a). Each channel in this WSS can be switched on or switched off, and the maximum extinction ratio is about 11 dB. The power consumption is 240 mW, while the average power consumption per ring is 16 mW. To demonstrate how we switch off part of channels, Fig. 10(b) shows the spectrum of the filter when the channels of No. 2, 6 and 11 are switched off. A more interesting case is shown in Fig. 10(c), where a WSS with a V-shape envelope is shown. It proves that the envelope of the switches can be changed as well. Obviously, the intervals of each channel can be changed as well due to the wavelength tunability. To show the performance of the filter as a band-pass filter, we

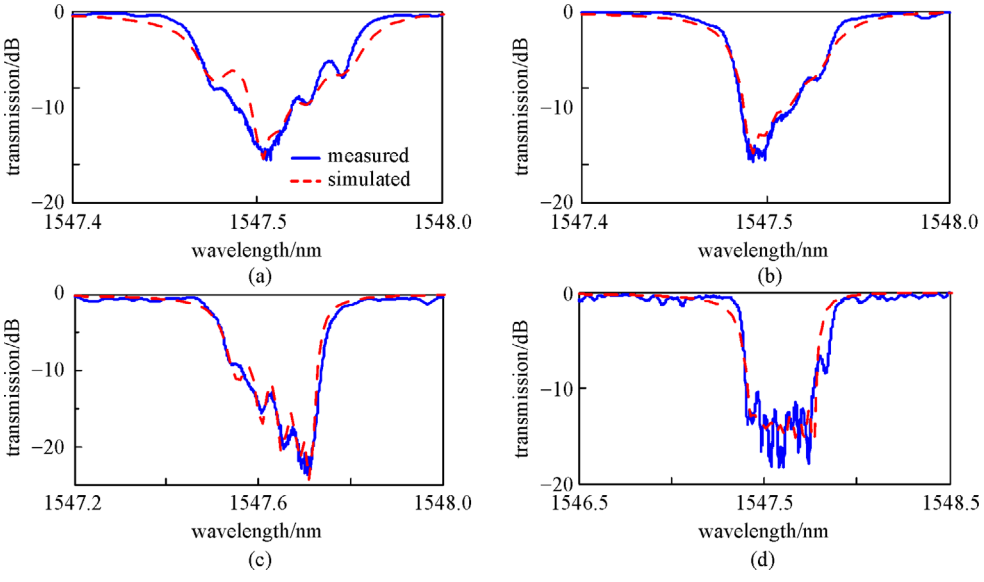

Fig. 8 Measured (blue solid line) and simulated (red dashed line) transfer functions in several specific shapes. (a) Isosceles triangle shape; (b) and (c) right angled triangle shape; (d) square shape

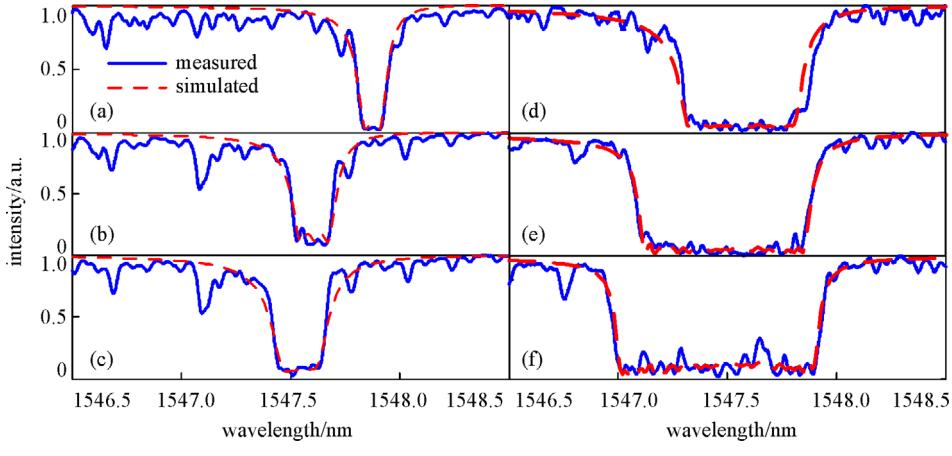

Fig. 9 Measured (blue solid line) and simulated (red dashed line) results for square shape transfer functions in different bandwidths. (a) 0.15 nm bandwidth; (b) 0.2 nm bandwidth; (c) 0.25 nm bandwidth; (d) 0.61 nm bandwidth; (e) 0.83 nm bandwidth; (f) 0.97 nm bandwidth

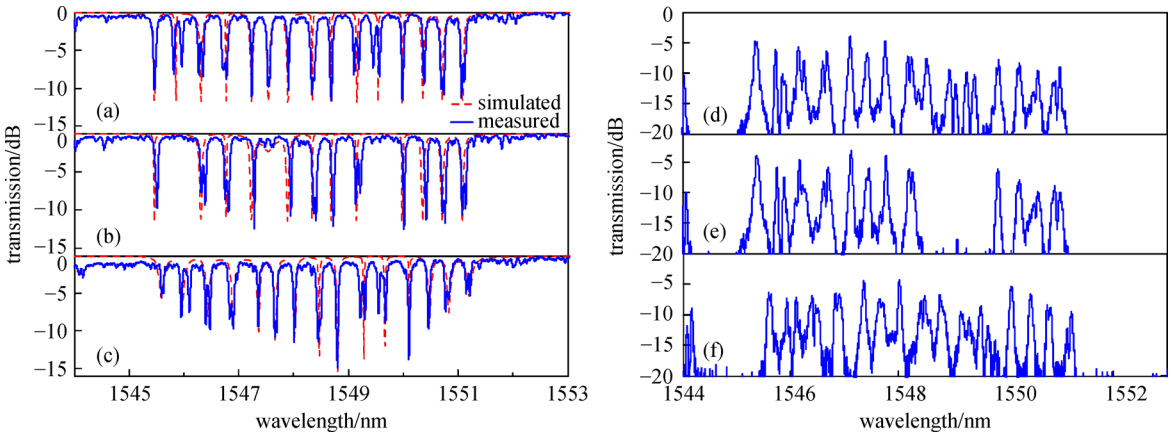

Fig. 10 Measured (blue solid line) and simulated (red dashed line) transfer functions of (a) wavelength selective switches, (b) wavelength selective switches with channel 2, 6 and 11 shut down, (c) wavelength selective switches with 'V' shape envelope; (d)–(f) corresponding drop-port transfer function of (a), (b) and (c)

provide the drop-port transfer function for each WSS, shown in Figs. 10(d) – 10(f). We can see that the passband spectrum is complementary to the notch spectrum, which indicates that our device can also serve as a band-pass filter. To sum up, the optical filter can obtain much wider bandwidth tuning range and free spectrum range (FSR) than our previous work [8]. The enlarged microring number also show higher reconfiguration than a single ring resonator [45].

4 Conclusions

In summary, we have proposed an on-chip integrated pulse processor employing cascaded MZI-MRR structure, making use of 32 micro-heaters divided into 16 MZI electrodes and 16 microring electrodes controlling the depth of spectral notches and central wavelength, respectively, thanks to the thermo-optic effect. Fabricated chip on SOI wafer can realize three functions. First, the chip can serve as a wide tunable differentiator with tuning range of 0.51 – 2.23 using 4 of all 16 rings with deviation no more than 7%. Then, it can also realize an optical filter whose shape and bandwidth are both tunable. In addition, a WSS is also demonstrated. The chip has 11 dB insertion loss, presenting a wide range of possibilities due to its on-chip integration, small footprint, low loss, low power consumption and wide reconfigurability.

Acknowledgements This work was supported by the National Natural Science Foundation of China (Grant Nos. 61475052 and 61622502).

References

1. Li M, Zhu N. Recent advances in microwave photonics. Frontiers of Optoelectronics, 2016, 9(2): 160–185
2. Capmany J, Novak D. Microwave photonics combines two worlds. Nature Photonics, 2007, 1(6): 319–330
3. Weiner A M. Ultrafast optical pulse shaping: a tutorial review. Optics Communications, 2011, 284(15): 3669–3692
4. Yao J. Photonic generation of microwave arbitrary waveforms. Optics Communications, 2011, 284(15): 3723–3736
5. Azaña J, Chen L R. Synthesis of temporal optical waveforms by fiber Bragg gratings: a new approach based on space-to-frequency-to-time mapping. Journal of the Optical Society of America B, Optical Physics, 2002, 19(11): 2758–2769
6. Leaird D E, Weiner A M. Femtosecond direct space-to-time pulse shaping in an integrated-optic configuration. Optics Letters, 2004, 29(13): 1551–1553
7. Shen M, Minasian R A. Toward a high-speed arbitrary waveform generation by a novel photonic processing structure. IEEE Photonics Technology Letters, 2004, 16(4): 1155–1157
8. Liao S, Ding Y, Peucheret C, Yang T, Dong J, Zhang X. Integrated programmable photonic filter on the silicon-on-insulator platform. Optics Express, 2014, 22(26): 31993–31998
9. Wang J, Shen H, Fan L, Wu R, Niu B, Varghese L T, Xuan Y, Leaird D E, Wang X, Gan F, Weiner A M, Qi M. Reconfigurable radio-frequency arbitrary waveforms synthesized in a silicon photonic chip. Nature Communications, 2015, 6(1): 5957
10. Weiner A M. Femtosecond pulse shaping using spatial light modulators. Review of Scientific Instruments, 2000, 71(5): 1929–1960
11. McKinney J D, Lin I S, Weiner A M. Shaping the power spectrum of ultra-wideband radio-frequency signals. IEEE Transactions on Microwave Theory and Techniques, 2006, 54(12): 4247–4255
12. Stowe M C, Pe'er A, Ye J. High resolution atomic coherent control via spectral phase manipulation of an optical frequency comb. In: Proceedings of 15th International Conference on Ultrafast Phenomena. Pacific Grove: Optical Society of America, 2006, MD8
13. Fontaine N K, Scott R P, Cao J, Karalar A, Jiang W, Okamoto K, Heritage J P, Kolner B H, Yoo S J B. 32 Phase X 32 amplitude optical arbitrary waveform generation. Optics Letters, 2007, 32(7): 865–867

14. Jiang Z, Huang C B, Leaird D E, Weiner A M. Optical arbitrary waveform processing of more than 100 spectral comb lines. Nature Photonics, 2007, 1(8): 463–467
15. Kyotoku B B C, Chen L, Lipson M. Sub-nm resolution cavity enhanced microspectrometer. Optics Express, 2010, 18(1): 102–107
16. Chou J, Han Y, Jalali B. Adaptive RF-photonic arbitrary waveform generator. IEEE Photonics Technology Letters, 2003, 15(4): 581–583
17. Dai Y, Chen X, Ji H, Xie S. Optical arbitrary waveform generation based on sampled fiber Bragg gratings. IEEE Photonics Technology Letters, 2007, 19(23): 1916–1918
18. Khan M H, Shen H, Xuan Y, Zhao L, Xiao S, Leaird D E, Weiner A M, Qi M. Ultrabroad-bandwidth arbitrary radiofrequency waveform generation with a silicon photonic chip-based spectral shaper. Nature Photonics, 2010, 4(2): 117–122
19. Bolea M, Mora J, Ortega B, Capmany J. Optical arbitrary waveform generator using incoherent microwave photonic filtering. IEEE Photonics Technology Letters, 2011, 23(10): 618–620
20. Zhang H, Zou W, Chen J. Generation of a widely tunable linearly chirped microwave waveform based on spectral filtering and unbalanced dispersion. Optics Letters, 2015, 40(6): 1085–1088
21. Yan S, Gao S, Zhou F, Ding Y, Dong J, Cai X, Zhang X. Photonic linear chirped microwave signal generation based on the ultra-compact spectral shaper using the slow light effect. Optics Letters, 2017, 42(17): 3299–3302
22. Ashrafi R, Dizaji M R, Cortés L R, Zhang J, Yao J, Azaña J, Chen L R. Time-delay to intensity mapping based on a second-order optical integrator: application to optical arbitrary waveform generation. Optics Express, 2015, 23(12): 16209–16223
23. Takenouchi H, Tsuda H, Naganuma K, Kurokawa T, Inoue Y, Okamoto K. Differential processing of ultrashort optical pulses using arrayed-waveguide grating with phase-only filter. Electronics Letters, 1998, 34(12): 1245–1246
24. Liao S, Ding Y, Dong J, Yang T, Chen X, Gao D, Zhang X. Arbitrary waveform generator and differentiator employing an integrated optical pulse shaper. Optics Express, 2015, 23(9): 12161–12173
25. Wang X, Zhou L, Li R, Xie J, Lu L, Wu K, Chen J. Continuously tunable ultra-thin silicon waveguide optical delay line. Optica, 2017, 4(5): 507
26. Liu Y, Choudhary A, Marpaung D, Eggleton B J. Gigahertz optical tuning of an on-chip radio frequency photonic delay line. Optica, 2017, 4(4): 418
27. Burla M, Marpaung D, Zhuang L, Roeloffzen C, Khan M R, Leinse A, Hoekman M, Heideman R. On-chip CMOS compatible reconfigurable optical delay line with separate carrier tuning for microwave photonic signal processing. Optics Express, 2011, 19 (22): 21475–21484
28. Efimov A, Reitze D H. Programmable dispersion compensation and pulse shaping in a 26-fs chirped-pulse amplifier. Optics Letters, 1998, 23(20): 1612–1614
29. Doerr C R, Marom D M, Cappuzzo M A, Chen E Y. 40-Gb/s colorless tunable dispersion compensator with 1000-ps/nm tuning range employing a planar lightwave circuit and a deformable mirror. In: Proceedings of Optical Fiber Communication Conference and Exposition and the National Fiber Optic Engineers Conference. Anaheim: Optical Society of America, 2005, PDP5
30. Weiner A M, Ferdous F, Wang P H, Leaird D E, Wang J, Fan L, Varghese L T, Niu B, Xuan Y, Qi M, Miao H, Srinivasan K, Chen L, Aksyuk V. Microresonator-based optical frequency combs: time-domain studies. In: Proceedings of Conference on Lasers and Electro-Optics. San Jose: Optical Society of America, 2012, FTh1G.1
31. Fontaine N K, Scott R P, Yoo S J B. Dynamic optical arbitrary waveform generation and detection in InP photonic integrated circuits for Tb/s optical communications. Optics Communications, 2011, 284(15): 3693–3705
32. Rasras M S, Kang I, Dinu M, Jaques J, Dutta N, Piccirilli A, Cappuzzo M A, Chen E Y, Gomez L T, Wong-Foy A, Cabot S, Johnson G S, Buhl L, Patel S S. A programmable 8-bit optical correlator filter for optical bit pattern recognition. IEEE Photonics Technology Letters, 2008, 20(9): 694–696
33. Zhang B, Zhang L, Yan L S, Fazal I, Yang J Y, Willner A E. Continuously-tunable, bit-rate variable OTDM using broadband SBS slow-light delay line. Optics Express, 2007, 15(13): 8317–8322
34. Supradeepa V R, Long C M, Wu R, Ferdous F, Hamidi E, Leaird D E, Weiner A M. Comb-based radiofrequency photonic filters with rapid tunability and high selectivity. Nature Photonics, 2012, 6(3): 186–194
35. Capmany J, Ortega B, Pastor D. A tutorial on microwave photonic filters. Journal of Lightwave Technology, 2006, 24(1): 201–229
36. Meijerink A, Roeloffzen C G H, Meijerink R, Zhuang L, Marpaung D A I, Bentum M J, Burla M, Verpoorte J, Jorna P, Hulzinga A, van Etten W. Novel ring resonator-based integrated photonic beamformer for broadband phased array receive antennas—part I: design and performance analysis. Journal of Lightwave Technology, 2010, 28(1): 3–18
37. Zhuang L, Roeloffzen C G H, Meijerink A, Burla M, Marpaung D A I, Leinse A, Hoekman M, Heideman R G, van Etten W. Novel ring resonator-based integrated photonic beamformer for broadband phased array receive antennas—part II: experimental prototype. Journal of Lightwave Technology, 2010, 28(1): 19–31
38. Wang C, Yao J. Large time-bandwidth product microwave arbitrary waveform generation using a spatially discrete chirped fiber Bragg grating. Journal of Lightwave Technology, 2010, 28(11): 1652–1660
39. Capmany J, Pastor D, Ortega B. New and flexible fiber-optic delay-line filters using chirped Bragg gratings and laser arrays. IEEE Transactions on Microwave Theory and Techniques, 1999, 47(7): 1321–1326
40. Marpaung D, Roeloffzen C, Heideman R, Leinse A, Sales S, Capmany J. Integrated microwave photonics. Laser & Photonics Reviews, 2013, 7(4): 506–538
41. Soares F M, Fontaine N K, Scott R P, Baek J H, Zhou X, Su T, Cheung S, Wang Y, Junesand C, Lourdudoss S, Liou K Y, Hamm R A, Wang W, Patel B, Gruezke L A, Tsang W T, Heritage J P, Yoo S J B. Monolithic InP 100-channel × 10-GHz device for optical arbitrary waveform generation. IEEE Photonics Journal, 2011, 3(6): 975–985
42. Tsuda H, Tanaka Y, Shioda T, Kurokawa T. Analog and digital optical pulse synthesizers using arrayed-waveguide gratings for

high-speed optical signal processing. Journal of Lightwave Technology, 2008, 26(6): 670–677
43. Zhang W, Yao J. Photonic generation of linearly chirped microwave waveform with a large time-bandwidth product using a silicon-based on-chip spectral shaper. In: Proceedings of 2015 International Topical Meeting on Microwave Photonics (MWP). Paphos: IEEE, 2015, 1–4
44. Yang R, Zhou L, Wang M, Zhu H, Chen J. Application of SOI microring coupling modulation in microwave photonic phase shifters. Frontiers of Optoelectronics, 2016, 9(3): 483–488
45. Xiao S, Khan M H, Shen H, Qi M. Silicon-on-insulator microring add-drop filters with free spectral ranges over 30 nm. Journal of Lightwave Technology, 2008, 26(2): 228–236
46. Zhuang L, Roeloffzen C G H, Hoekman M, Boller K J, Lowery A J. Programmable photonic signal processor chip for radiofrequency applications. Optica, 2015, 2(10): 854–859
47. Liu W, Li M, Guzzon R S, Norberg E J, Parker J S, Lu M, Coldren L A, Yao J. A fully reconfigurable photonic integrated signal processor. Nature Photonics, 2016, 10(3): 190–195
48. Xie Y, Zhuang L, Lowery A J. Picosecond optical pulse processing using a terahertz-bandwidth reconfigurable photonic integrated circuit. Nanophotonics, 2018, 7(5): 837–852
49. Zhang W, Yao J. A fully reconfigurable waveguide Bragg grating for programmable photonic signal processing. Nature Communications, 2018, 9(1): 1396
50. Xue X, Xuan Y, Kim H J, Wang J, Leaird D E, Qi M, Weiner A M. Programmable single-bandpass photonic RF filter based on Kerr comb from a microring. Journal of Lightwave Technology, 2014, 32 (20): 3557–3565
51. Chen L, Sherwood-Droz N, Lipson M. Compact bandwidth-tunable microring resonators. Optics Letters, 2007, 32(22): 3361–3363
52. Liu M, Zhao Y, Wang X, Zhang X, Gao S, Dong J, Cai X. Widely tunable fractional-order photonic differentiator using a Mach–Zenhder interferometer coupled microring resonator. Optics Express, 2017, 25(26): 33305
53. Cuadrado-Laborde C. All-optical ultrafast fractional differentiator. Optical and Quantum Electronics, 2008, 40(13): 983–990
54. Berger N K, Levit B, Fischer B, Kulishov M, Plant D V, Azaña J. Temporal differentiation of optical signals using a phase-shifted fiber Bragg grating. Optics Express, 2007, 15(2): 371–381
55. Orlandi P, Morichetti F, Strain M J, Sorel M, Bassi P, Melloni A. Photonic integrated filter with widely tunable bandwidth. Journal of Lightwave Technology, 2014, 32(5): 897–907

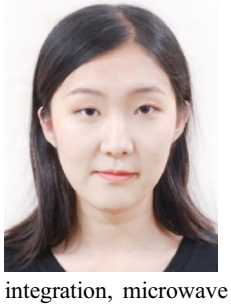

Yuhe Zhao is a doctoral student majored in optical engineering in Wuhan National Laboratory for Optoelectronics, Huazhong University of Science and Technology (HUST), Wuhan, China, where she joined the Optoelectronic Devices and Integration Laboratory. She received her bachelor's degree from HUST in 2016. Her research interests are optoelectronic devices and integration, microwave photonics and arbitrary waveform generation.

Xu Wang receiced her bachelor's degree in 2014 and is currently a doctoral student majored in optical engineering in Wuhan National Laboratory for Optoelectronics, Huazhong University of Science and Technology (HUST), Wuhan, China. Her current work lies in optoelectronic devices and integration and microwave frequency measurement.

Dingshan Gao is an associate professor in Wuhan National Laboratory for Optoelectronics, Huazhong University of Science and Technology (HUST), Wuhan, China. He received the B.S. degree from Wuhan University of Technology (WHUT), China in 2000, and Ph.D. degree in Institute of Semiconductors (IOS), Chinese Academy of Sciences (CAS). He is working on quantum optics, nonlinear optics, nano optics and optoelectronic devices and integration technology.

Jianji Dong is a professor in Wuhan National Laboratory for Optoelectronics, Huazhong University of Science and Technology (HUST), Wuhan, China. He received his Ph.D. degree in optoelectronics engineering from HUST in 2008. From Feb. 2006 to Aug. 2006, he worked in Network Technology Research Centre (NTRC), Nanyang Technological University, Singapore, as an exchange student. From Nov. 2008 to Feb. 2010, he worked in Centre of Advanced Photonics and Electronics, Cambridge University as a research associate. He is working on the silicon photonics, photonic computing, and microwave photonics.

Xinliang Zhang received the B.S. and Ph.D. degrees from Huazhong University of Science and Technology (HUST), China, in 1992 and 2001. He became a full professor of School of Optical and Electronic Information, HUST in 2004, and now he is also a full professor of Wuhan National Laboratory for Optoelectronics (WNLO). Currently, he is the dean of School of Optical and Electronic Information, HUST, and also the director of Division of Optoelectronic Devices and Integration (OEDI) in WNLO. His research areas cover semiconductor optoelectronic devices for optical interconnection and optical signal processing.